

RoSIS: Robust Framework for Text-Promptable Surgical Instrument Segmentation Using Vision-Language Fusion

Tae-Min Choi, and Juyoun Park, *Member, IEEE*

Abstract—Surgical instrument segmentation (SIS) is an essential task in computer-assisted surgeries, with deep learning-based research improving accuracy in complex environments. Recently, text-promptable segmentation methods have been introduced to generate masks based on text prompts describing target objects. However, these methods assume that the object described by a given text prompt exists in the scene. This results in mask generation whenever a related text prompt is provided, even if the object is absent from the image. Existing methods handle this by using prompts only for objects known to be present in the image, which introduces inaccessible information in a vision-based method setting and results in unfair comparisons. For fair comparison, we redefine existing text-promptable SIS settings to robust conditions, called Robust text-promptable SIS (R-SIS), designed to forward prompts of all classes and determine the existence of an object from a given text prompt for the fair comparison. Furthermore, we propose a novel framework, Robust Surgical Instrument Segmentation (RoSIS), which combines visual and language features for promptable segmentation in the R-SIS setting. RoSIS employs an encoder-decoder architecture with a Multi-Modal Fusion Block (MMFB) and a Selective Gate Block (SGB) to achieve balanced integration of vision and language features. Additionally, we introduce an iterative inference strategy that refines segmentation masks in two steps: an initial pass using name-based prompts, followed by a refinement step using location prompts. Experiments on various datasets and settings demonstrate that RoSIS outperforms existing vision-based and promptable methods under robust conditions.

Index Terms—Surgical instrument segmentation, Robust text-promptable surgical instrument segmentation, Referring image segmentation, Instance segmentation, Computer vision

I. INTRODUCTION

AS minimally invasive surgeries [1], [2] have been increasingly adopted due to their various advantages, surgeons now rely on camera-captured views to perform procedures, as they cannot directly see the surgical site. Surgical Instrument

Segmentation (SIS) [3] has gained attention as a fundamental technology required to assist surgeons in this surgical vision environment. Various vision-based deep learning methods [4]–[9] have achieved impressive performance. However, due to the characteristics of SIS, these methods often rely on datasets of limited scale, resulting in insufficient performance, and they lack the capability in terms of human-robot interaction for robot-assisted surgeries. Recently, language and vision-language model-based methods [10], [11] have been developed to overcome these challenges. They introduced a new approach to SIS called text-promptable surgical instrument segmentation [10] based on Referring Image Segmentation (RIS) [12], [13].

RIS generates an object mask based on a given text description. However, RIS methods typically assume that the object described by the text exists within the image. When an incorrect or unrelated text is provided, the model produces a mismatched mask. To address this issue, Generalized Referring Expression Segmentation (GRES) [14] and Robust Referring Image Segmentation (R-RIS) [15] have been proposed. These methods first classify whether the object described by the text actually exists in the image. If the object is present, they proceed to predict the mask.

A similar issue arises in RIS-based text-promptable SIS methods. These methods define a text sentence by utilizing the instrument’s name along with a detailed description generated from the large language model such as GPT-4 [16]. They then predict a mask that corresponds to the given instrument prompt. However, even when a text prompt for an instrument that is not present in the image is provided, the model still produces an incorrect mask. Existing methods handle this by first identifying the instruments in the image and then providing prompts only for those that are detected. However, it utilizes inaccessible information (the existence of an object) in the evaluation phase, causing an unfair comparison with vision-based models.

Accordingly, inspired by the R-RIS [15] approach, we redefine the text-promptable SIS under robust conditions as called Robust text-promptable Surgical Instrument Segmentation (R-SIS). As illustrated in Fig. 1, previous promptable SIS models [10], [11], [17] use prompts only for categories present within the image, which is inaccessible information in the vision-based models. They generate segmentation maps for a subset of classes because they only use prompts for objects in the image. Unlike previous approaches, R-SIS

This work was supported by the Technology Innovation Program (RS-2024-00443054, Development of a Supermicrosurgical Robot System for Sub-0.8mm Vessel Anastomosis through Human-Robot Autonomous Collaboration in Surgical Workflow Recognition) funded By the Ministry of Trade Industry & Energy(MOTIE, Korea).

Tae-Min Choi and Juyoun Park are with Center for humanoid research, Korea Institute of Science Technology (KIST), Seoul, South Korea (e-mail: tmchoi@kist.re.kr; juyounpark@kist.re.kr).

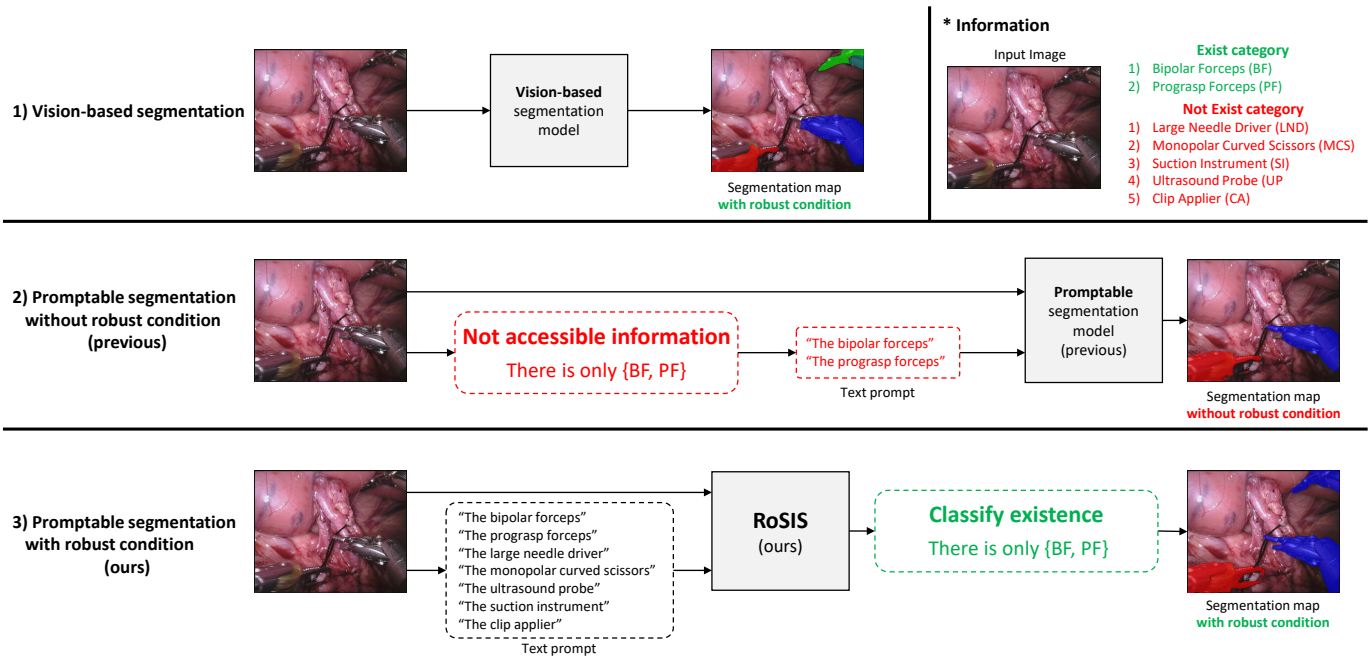


Fig. 1. Comparison of surgical instrument segmentation method: (1) Vision-based segmentation model only uses the image and generates all classes of segmentation maps; (2) Previous promptable segmentation model uses “not accessible information” to identify categories present in the image and generates segmentation maps only for those categories. This means they are led to settings without robust conditions; (3) Our robust promptable segmentation model uses prompts for all classes, generating segmentation maps for all categories under robust conditions.

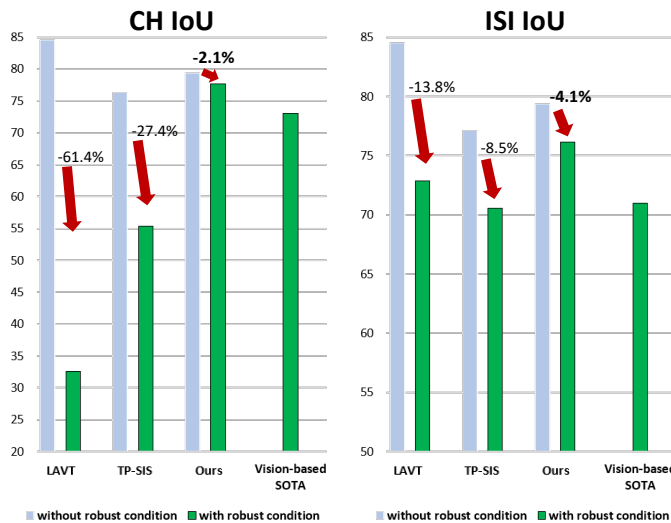


Fig. 2. Performance comparison on the EndoVis2018 dataset under with and without robust conditions. Existing models exhibit significant performance degradation, with dramatic drops in both Challenge IoU (Ch IoU) and ISI IoU. In contrast, our robust promptable segmentation model demonstrates minimal performance degradation across both metrics and outperforms the vision-based SOTA method (ISINet).

ensures a fair comparison by incorporating text prompts for all categories within the dataset, regardless of their presence in the image. To achieve this robustness, R-SIS employs negative prompts for non-existing objects and positive prompts for existing objects in training, enabling the model to classify each object’s presence or absence effectively. This strategy avoids false positives and improves accuracy in diverse and realistic surgical scenarios. To support the development and

evaluation of R-SIS, we build the dataset for R-SIS using the EndoVis2017 [18] and EndoVis2018 [19] datasets. This adapted dataset includes comprehensive prompts for R-SIS, facilitating more reliable training and evaluation under robust conditions.

Previous promptable SIS methods assume the presence of an object matching the given text, which results in increased false positives in the R-SIS environment. As shown in Fig. 2, previous methods suffer from significant performance degradation when evaluated under robust conditions. There are even cases where the performance is lower than that of vision-based methods that do not use language information. To address this limitation, we propose a novel framework designed to perform well in robust conditions. Our model, named **Robust Surgical Instrument Segmentation (RoSIS)**, includes two key modules: the **Multi-Modal Fusion Block (MMFB)** and the **Selective Gate Block (SGB)**. The MMFB effectively integrates visual and language features to enhance contextual understanding with language tokens, while the SGB dynamically adjusts the balance of visual and fused features. We also propose the **iterative inference** to generate more accurate segmentation maps at test time. Iterative inference produces a refined map through two iterations: the first iteration uses prompts based on the object name and a generative model, while the second iteration incorporates location prompts generated using the initial map. This architecture and strategy enable RoSIS to achieve stable and accurate segmentation across a broad range of surgical conditions.

Our model demonstrates competitive performance on the EndoVis2017 and EndoVis2018, achieving powerful results to vision-based models under robust evaluation conditions. To ensure this robustness, we carefully revisit our experimental

process, allowing for precise benchmarking. Additionally, we conduct comparisons with existing promptable methods under the R-RIS setting to further validate our approach. This thorough evaluation shows the robustness and effectiveness of our model, highlighting its ability to maintain high accuracy and reliability, even when directly compared with vision-based and promptable segmentation methods.

II. RELATED WORKS

A. Surgical Instrument Segmentation

Surgical instrument segmentation (SIS) involves predicting the pixel-wise regions of instruments in surgical images. Early research [4], [7]–[9], [20] in this field applied image-based segmentation methods to address SIS. TeraNet [4] marked the beginning of deep learning-based approaches by introducing a modified U-Net [21] architecture based semantic segmentation framework with pre-trained VGG11/VGG16 encoders and skip connections for precise location. ISINet [7], employing a Mask R-CNN [22] architecture, incorporates a novel temporal consistency module to track and correct instrument predictions across video frames. TraSeTR [20] utilizes a Track-to-Segment Transformer architecture, combining query embeddings with contrastive learning to ensure robust tracking and segmentation across video frames. MATIS [9], a video-based SIS method, leverages a two-stage structure with Mask2Former [23] to generate and classify region proposals using masked and deformable attention and video transformers to maintain temporal consistency. S3Net [8] builds on Mask R-CNN [22] with a three-stage architecture, adding a Multi-Scale Mask-Attended classifier to refine class predictions based on mask-attended features, improving instance segmentation of surgical instruments. Recently, with the development of segmentation techniques that utilize information beyond vision, promptable segmentation models that use external prompts, such as text or prototypes, have been proposed for SIS.

SurgicalSAM [17] proposes an efficiently fine-tuning method for Segment Anything Model (SAM) [24]. SAM is a segmentation model using prompts (points, bounding boxes, or text inputs) from prompt encoder. Since SAM was originally designed for natural domain image segmentation, SurgicalSAM adapts SAM for the surgical domain, making it suitable for SIS. Additionally, SurgicalSAM introduces a prototype-based class prompt encoder that generates prompt embeddings for each class, which are then used as SAM prompts. Later, various text-promptable SIS methods were proposed, leveraging vision-language models (VLM) to use text prompts for segmentation tasks. SP-SAM [11] uses SAM [24] as its baseline and incorporates both category-level and part-level text prompts as prompt embeddings. TP-SIS [10], a method based on CLIP [25], utilizes text prompts describing instruments, which are categorized into name-based prompts, CLIP’s prompt templates, and prompts generated from GPT-4 [16]. Although these methods have been proposed for text-promptable SIS, they are trained and inferred with the assumption that the object described by the text expression exists within the image. As a result, their performance degrades significantly when a text prompt refers to an object not present

in the image. In this paper, we address this issue by adopting a robust referring image segmentation [15] approach for text-promptable SIS. We first determine the existence of the object to reduce false positives and handle negative expressions. Furthermore, we resolve the unfair comparisons that occur in existing text-promptable segmentation models, ensuring a fair comparison with vision-based segmentation models.

B. Referring Image Segmentation

Referring Image Segmentation (RIS) aims to segment the object corresponding to a given text expression. MAttNet [13] designs a language attention network using word embeddings and an LSTM, then compares these with object proposals to generate a mask that matches the expression. VLT [26] and EFN [27] propose a Bi-GRU language model and a ResNet-based image backbone to generate features fused in the decoder through multi-modal information integration. With the development of Vision Transformers (ViT) [28], various methods are applied ViT to RIS tasks. LAVT [12] introduced an early fusion method that combines text features generated by BERT [29] with visual features from ViT through pixel-word attention, achieving significant performance improvements.

However, previous works assumed that each expression must always match an object, which led to the crucial issue of generating incorrect masks for expressions that do not correspond to any object in the image. ReLA [14] overcomes this by proposing Generalized Referring Expression Segmentation, incorporating empty-target (no target for given text) and multi-target annotations (multiple targets for given text). RefSegformer [15] focuses on the empty-target scenario, proposing a robust referring image segmentation approach. The empty-target problem also arises in existing promptable surgical instrument segmentation methods, and we aim to address this issue in our work.

III. METHOD

This section presents our approach to robust text-promptable surgical instrument segmentation (R-SIS). Section III-A formulates the problem for R-SIS, identifying key challenges in promptable segmentation for surgical instruments. Section III-B defines the construction of text prompts used for training, detailing the use of descriptive prompts to enhance model understanding. Section III-C describes the model architecture, including the encoder-decoder structure and multi-modal fusion components. Finally, Section III-C.2 introduces an iterative inference strategy aimed at refining mask accuracy through repeated inference steps.

A. Problem formulation

Surgical instrument segmentation (SIS) is the task of segmenting surgical tools in an endoscopic surgery image $I \in \mathbb{R}^{H \times W \times 3}$, where H and W denote the height and width of the image, respectively. For text-promptable SIS, we incorporate an image I and a text prompt T containing the names or attributes of the surgical tools, making the segmentation task responsive to specific prompts.

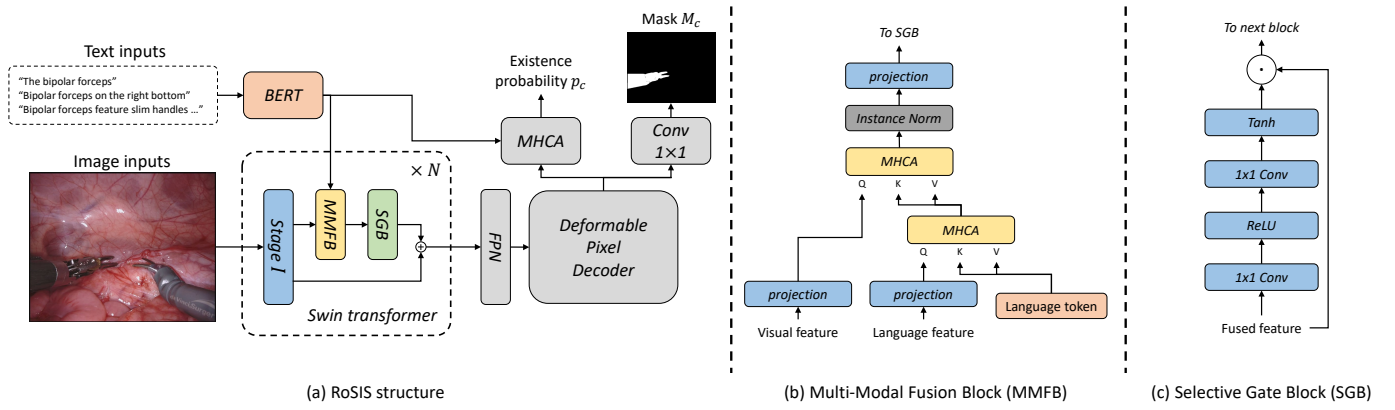


Fig. 3. RoSIS model architecture with (a) overall structure, (b) Multi-Modal Fusion Block (MMFB), and (c) Selective Gate Block (SGB).

In traditional vision-based SIS, the model takes only image I as input and predicts a mask $M \in \mathbb{R}^{H \times W \times C}$ that includes C classes, each corresponding to a specific surgical instrument. However, in text-promptable SIS, both the image I and a class-specific text prompt t_c are provided as input for each class c . This enables the model to generate a binary mask $M_c \in \mathbb{R}^{H \times W \times 1}$ for each class c . For the robust text-promptable surgical instrument segmentation (R-RIS), we also generate an existence probability p_c , which classifies the class c in the image for a given text prompt t_c .

In the test phase, we conduct inference across all C classes for a given image I , resulting in class-specific masks M_1, \dots, M_C and existence probabilities p_1, \dots, p_C . These outputs are then aggregated to the final mask $M \in \mathbb{R}^{H \times W \times C}$, with each pixel in M representing the class-specific segmentation.

To ensure R-SIS, we incorporate existence probabilities, allowing our model to assess the presence of each instrument class first. This setup enables to avoidance of producing unnecessary masks for absent classes, reducing false positives, and enhancing segmentation accuracy under the R-SIS setting. By integrating class existence probabilities, our method is evaluated under robust conditions with vision-based models and demonstrates results under practical conditions.

B. Prompt generation

There are various ways to create text prompts t_c for each class c . Following the approach in TP-SIS [10], we generate prompts using the class name, such as “The {cls name}” and we utilize GPT-4 [16] to generate detailed prompts describing each class’s visual characteristics. This combination provides both general and specific prompts, enabling the model to recognize instruments based on both name and appearance.

Since surgical instruments often appear in consistent positions on the screen during surgery, we further enhance the prompts by designing location-based descriptions. To do this, we calculate the center of mass for each instrument’s ground truth mask to identify its typical position, creating prompts like “The {cls name} on the {location}.” For location prompts, we categorize positions into four options: “left-top,” “left-bottom,” “right-top,” and “right-bottom.” During model training, we employ all three types of text prompts—class name prompt,

GPT-4 visual prompt, and location prompt—for each class c , ensuring comprehensive contextual information.

If training only with positive prompts (describing objects present in the image), the model may develop a bias toward the presence of instruments, potentially reducing generalization [15]. To counter this, we also generate negative prompts for classes absent from the image, thus enhancing the classification ability to distinguish between existing and non-existing classes. For absent classes, we create prompts using both the class name and GPT-4 description prompts, as well as a randomly selected location prompt from the four options, to provide a full range of negative examples. We balance the positive and negative prompts corresponding to one image for stable training.

C. Architecture

We design our *Robust Surgical Instrument Segmentation (RoSIS)* using an encoder-decoder structure to achieve robust text-promptable surgical instrument segmentation. Inspired by [15] and [14], we add a binary classifier in parallel with the decoder to determine the existence of instruments. First, we encode the image I and text description T using an image encoder and a text encoder, respectively. The image encoder is based on the Swin Transformer [30], which is specialized for dense prediction tasks, while the text encoder uses BERT [29]. We denote the visual feature from stage i of the Swin Transformer as $v_i \in \mathbb{R}^{H_i \times W_i \times C_i}$ and the language feature from BERT as $l \in \mathbb{R}^{T \times C_l}$, where H_i and W_i are the height and width of the visual feature, T is the number of words in the text description, and C_i and C_l represent the number of channels for the visual and language features, respectively.

1) *Encoder design*: We introduce early feature fusion to efficiently integrate vision and language knowledge from the encoder. We aim to enhance semantic understanding and improve feature interactivity through early fusion. For this purpose, we add the *Multi-Modal Fusion Block (MMFB)* and the *Selective Gate Block (SGB)* between each stage of the Swin Transformer.

Fig. 3(b) shows the architecture of the MMFB, which is designed to integrate visual and language features through a multi-step fusion process, with the fused feature then passed to a gating module. The fusion process begins by independently

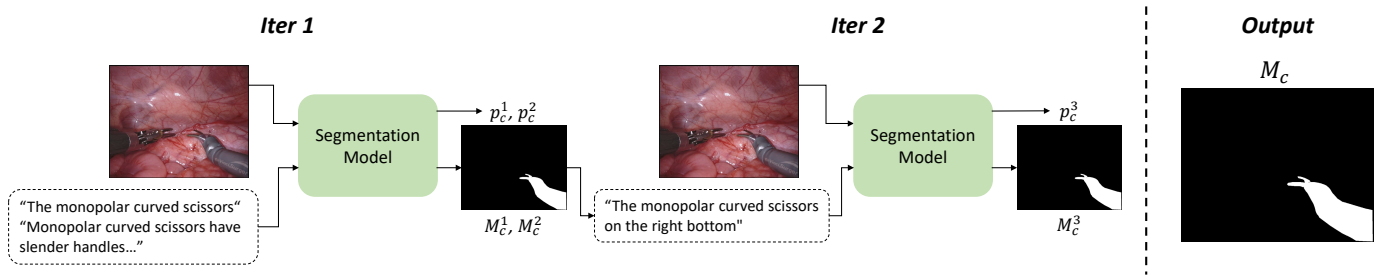


Fig. 4. Iterative segmentation process: (Iteration 1) initial segmentation using a general prompt, (Iteration 2) refined segmentation with a location prompt referring to the first predicted map. Then, we combine maps by equation 4 for accurate final output.

projecting the visual and language features into compatible feature spaces. The MMFB contains two Multi-Head Cross Attention (MHCA) modules. In the first MHCA, we adopt language tokens to fuse with the language feature. Unlike [15], since we do not use the language features generated during fusion in the decoder, we focus on selecting only the information necessary for fusion with visual features. Therefore, we refine the language features with one MHCA and subsequently use them in the second MHCA to interact with the visual features.

Inspired by [12], after the MMFB, we introduce the SGB to regulate the flow of fused features, ensuring that language features do not dominate the visual information. The SGB dynamically controls feature importance, allowing the model to maintain a balanced representation of both visual and language features before passing them to the next stage. As shown in Fig. 3(c), the SGB takes the fused feature as input, processes it through a series of lightweight transformations and applies a gating mechanism.

The whole fusion process between each stage are formulated as follows:

$$v_i = V_i(f_{i-1}), \quad i \in \{1, 2, 3, 4\} \quad (1)$$

$$f_i = \begin{cases} v_i + \text{SGB}_i(\text{MMFB}_i(v_i, l)), & i \in \{1, 2, 3, 4\}, \\ I, & i = 0 \end{cases} \quad (2)$$

where V_i represents the i -th stage of the Swin Transformer, and SGB_i and MMFB_i denote the i -th fusion blocks placed between V_i and V_{i+1} . We describe the effects of the encoder fusion architecture in the ablation study in Table III.

2) Decoder design: Our decoder is designed to perform two tasks: classify the existence of the object specified by the text prompt and generate the corresponding segmentation mask. To accomplish this, we use a multi-scale deformable attention pixel decoder [31]. This decoder incorporates an FPN [32] structure to effectively utilize multi-scale features, taking f_1, f_2, f_3 , and f_4 as inputs. The final segmentation mask M_c is produced to pass the output from the decoder through a 1×1 convolution layer.

In addition to mask generation, we introduce a parallel branch to compute the existence probability of the object described by the text prompt. This branch fuses the decoder output from f_4 with the raw language feature extracted from BERT using MHCA. This fusion enables the decoder to leverage both visual and textual information, enhancing its ability to determine the presence of the specified object. Unlike

[15], which uses fused language features from the encoder for existence prediction, we use the raw language feature directly from BERT, as it retains richer semantic context. After the fusion through MHCA, the existence probability p_c is computed by passing the output through a linear layer.

Finally, we calculate the cross-entropy loss for both the generated mask and the existence probability to optimize the model’s accuracy in both segmentation and existence detection tasks, shown as follows:

$$L = \text{BCELoss}(p_c, y_c) + \lambda \cdot \text{CELoss}(M_c, M_c^{gt}) \quad (3)$$

where λ is a hyperparameter for mask loss, y_c and M_c^{gt} denote the ground truth of the existence and the mask of class c , respectively.

D. Iterative inference

We propose an *iterative inference* strategy to use location prompts during inference, similar to those used in training. In the training phase, we can generate location prompts because we have access to the ground truth for the instrument, but this is not possible in the inference phase. Therefore, as shown in Fig. 4, we divide the inference process into two iterations.

In the first iteration, we generate the initial segmentation map and existence probability for each instrument category. We use two prompts: a category name prompt (e.g., “The monopolar curved scissors”) and a descriptive prompt generated by GPT, which provides visual characteristics of the instrument. For category c , the model predicts the segmentation maps M_c^1 and M_c^2 and the existence probabilities p_c^1 and p_c^2 . If the average existence probability $(p_c^1 + p_c^2)/2$ exceeds 0.5, indicating that class c exists in the image, the process proceeds to the second iteration.

In the second iteration, spatial information is used to refine the segmentation. Based on the segmentation maps M_c^1 and M_c^2 from the first iteration, the model calculates the center of mass for the detected object, allowing it to determine a rough location within one of four quadrants: left-top, left-bottom, right-top, or right-bottom. This positional information is then incorporated into a new location prompt (e.g., “The monopolar curved scissors on the right bottom”), which serves as input for the second inference. The model generates the segmentation map M_c^3 and the existence probability p_c^3 for the class c .

TABLE I

COMPARISON BETWEEN OUR RoSIS WITH THE PREVIOUS VISION-BASED AND PROMPTABLE METHOD ON THE ENDOVIS2018 DATASET. * MEANS RE-IMPLEMENTED RESULTS. † MEANS THAT DOES NOT UTILIZE CATEGORY EXISTENCE INFORMATION IN THE IMAGE DURING INFERENCE.

Domain	Method	Robustness [†]	Ch IoU	ISI IoU	mc IoU	Instrument category						
						BF	PF	LND	SI	CA	MCS	UP
Vision	TernausNet-11 [4]	✓	46.22	39.87	14.19	44.20	4.67	0.00	0.00	0.00	50.44	0.00
	MF-TAPNet [5]	✓	67.87	39.14	24.68	69.23	6.10	11.68	14.00	0.91	70.24	0.57
	Dual-MF [6]	✓	70.40	-	35.09	74.10	6.80	46.00	30.10	7.60	80.90	0.00
	ISINet [7]	✓	73.03	70.97	40.21	73.83	48.61	30.98	37.68	0.00	88.16	2.16
	S3Net [8]	✗	<u>75.81</u>	<u>74.02</u>	<u>42.58</u>	<u>77.22</u>	50.87	19.83	50.59	0.00	92.12	<u>7.44</u>
Promptable	LAVT* [12]	✓	72.87	32.58	25.97	77.19	10.96	8.79	16.47	2.78	64.04	1.55
	RefSegformer [15]	✓	77.09	68.67	36.70	80.67	20.88	25.06	38.86	0.10	86.23	5.13
	TP-SIS* [10]	✓	70.55	55.37	29.93	72.12	12.33	15.66	20.56	1.98	85.56	1.30
	RoSIS (ours)	✓	77.66	76.16	44.54	84.11	42.73	<u>35.26</u>	<u>46.36</u>	0.00	88.10	15.22

TABLE II

COMPARISON BETWEEN OUR RoSIS WITH THE PREVIOUS VISION-BASED AND PROMPTABLE METHOD ON THE ENDOVIS2017 DATASET. * MEANS RE-IMPLEMENTED RESULTS. † MEANS THAT DOES NOT UTILIZE CATEGORY EXISTENCE INFORMATION IN THE IMAGE DURING INFERENCE.

Domain	Method	Robustness [†]	Ch IoU	ISI IoU	mc IoU	Instrument category						
						BF	PF	LND	VS	GR	MCS	UP
Vision	TernausNet-11 [4]	✓	35.27	12.67	10.17	13.45	12.37	20.51	5.97	1.08	1.00	16.76
	MF-TAPNet [5]	✓	37.35	13.49	10.77	16.39	14.11	19.01	8.11	0.31	4.09	13.40
	Dual-MF [6]	✓	45.80	-	26.40	34.40	21.50	64.30	24.10	0.80	17.90	21.80
	ISINet [7]	✓	55.62	52.20	28.96	38.70	38.50	50.09	27.43	2.01	28.72	12.56
	S3Net [8]	✗	72.54	71.99	46.55	75.08	54.32	<u>61.84</u>	35.50	27.47	<u>43.23</u>	28.38
Promptable	LAVT* [12]	✓	37.57	11.10	10.90	17.05	12.97	14.25	11.91	2.23	7.98	9.90
	RefSegformer [15]	✓	46.58	32.81	27.87	33.37	0.30	52.69	38.50	0.03	37.05	33.14
	TP-SIS* [10]	✓	51.36	46.64	31.24	43.81	27.70	46.42	41.25	3.98	46.83	8.70
	RoSIS (ours)	✓	<u>63.07</u>	<u>57.33</u>	<u>40.65</u>	<u>67.34</u>	<u>39.95</u>	55.85	45.32	<u>5.10</u>	26.00	44.99

For the final output M_c , the segmentation maps from both iterations are combined using as below:

$$M_c = \begin{cases} 0, & \text{if } \frac{p_c^1 + p_c^2}{2} < 0.5 \\ \frac{M_c^1 + M_c^2}{2}, & \frac{p_c^1 + p_c^2}{2} \geq 0.5 \ \& \ p_c^3 < 0.5 \\ \frac{M_c^1 + M_c^2 + M_c^3}{3}, & \frac{p_c^1 + p_c^2}{2} \geq 0.5 \ \& \ p_c^3 \geq 0.5 \end{cases} \quad (4)$$

This combination leverages both the fixed prompts and the location prompt, resulting in a more precise and contextually aware segmentation map. This iterative inference approach ensures robust segmentation by progressively refining predictions based on both textual and spatial prompts, enhancing segmentation performance in complex surgical images. We describe the effects of iterative inference in detail in the ablation study in Table V.

IV. EXPERIMENT

A. Dataset and metric

We evaluate our method using the EndoVis2017 [18] and EndoVis2018 [19] datasets based on endoscopic surgery videos. The EndoVis2017 dataset consists of 10 videos recorded using the da Vinci surgical robot system, each containing 255 frames. This dataset includes seven classes: bipolar forceps (BF), prograsp forceps (PF), large needle driver (LND), vessel sealer (VS), grasping retractor (GR), monopolar curved scissors (MCS), and ultrasound probe (UP). Following [3], we apply 4-fold cross-validation to assess performance. The EndoVis2018 dataset consists of 15 videos, divided into 11 training and 4 test video sequences, and includes the

following seven classes: bipolar forceps, prograsp forceps, large needle driver, monopolar curved scissors, ultrasound probe, suction instrument (SI), and clip applicator (CA). The EndoVis2018 dataset exhibits severe class imbalance in the training set, and to ensure balanced learning, we adjust class frequencies within the dataloader.

We follow the evaluation metrics used in previous works [7], [10], which include Challenge IoU (Ch IoU), ISI IoU, and mean class IoU (mc IoU). Ch IoU calculates the IoU for classes present in the image and then computes the average. ISI IoU measures the IoU across all classes, while mc IoU represents the average IoU for each class.

B. Implementation detail

We implement our model using PyTorch [33]. For the language model, we utilize a pre-trained BERT [29]. The image encoder is initialized with an ImageNet [34] pre-trained Swin Transformer [30] to support dense prediction. In our fusion module, we set the language query size to 20. The model is trained using the AdamW [35] optimizer with a weight decay of 0.01 for 50 epochs, applying a learning rate decay of 0.1 at epochs 30 and 40. The input images, originally sized at 1280×1024, are resized to 480×480 for training, and the generated masks are upsampled to their original size to produce the final mask. We train the model with a batch size of 32, using four Nvidia RTX A6000 GPUs.

TABLE III

TEXT PROMPT DESIGN AND ITERATIVE INFERENCE ABLATION STUDY IN ENDOVIS2018 DATASET.

	ISI IoU	mc IoU
Name prompt	67.74	37.84
(+) location prompt	69.24 (+1.50)	37.54 (-0.30)
(+) Iterative inference	73.51 (+5.77)	39.30 (+1.46)
(+) gpt4 prompt	71.37 (+3.63)	40.61 (+2.77)
(+) Iterative inference	76.16 (+8.42)	44.54 (+6.70)

C. Results

1) *Comparison on the EndoVis2018*: In Table I, we compare our method, RoSIS, with both vision-based and promptable models on the EndoVis2018 [19] dataset. For a fair comparison, we re-implement the promptable models LAVT [12] and TP-SIS [10], both of which are based on referring image segmentation tasks. For promptable methods, we provide referring sentences for all classes in the EndoVis2018 dataset, where the number of classes is fixed to seven. Pixel-wise probabilities of the generated masks were then compared to produce the final output. To ensure robustness, the vision-based models were restricted to single-image methods instead of based on the video input methods. However, S3Net is not robust because it measures the performance by selecting the top 5 instances out of 7 instances during inference. Therefore, in Table I and II, we add the 'Robustness' column to indicate that S3Net has the advantage in the inference stage.

As shown in Table I, our method, RoSIS, not only outperforms all promptable models but also achieves superior performance compared to vision-based methods across the Ch IoU, ISI IoU, and mc IoU metrics. Vision-based models, while effective in standard segmentation tasks, do not leverage text prompts and therefore lack the adaptability provided by RoSIS's robust promptable framework. Our method performs better even though S3Net has an advantage by limiting the number of instances during inference, with a performance improvement of +2.44% in Ch IoU and +2.89% in ISI IoU and 4.60% in mc IoU. Promptable models, such as LAVT and TP-SIS, also tend to generate a high number of false negatives, as they produce masks without first determining whether the instrument is present in the image. This limitation results in a significant gap between Ch IoU and ISI IoU scores. In contrast, our model demonstrates more stable performance by first assessing the existence of each object, effectively reducing false negatives and achieving higher segmentation accuracy.

2) *Comparison on the EndoVis2017*: Table II presents a comparison between our method, RoSIS, and previous vision-based and promptable methods on the EndoVis2017 [18] dataset. Among the vision-based methods, S3Net [8] achieves the highest performance, surpassing our model on this dataset. However, S3Net's inference stage is limited by a selective approach in which it only considers the top 5 instances, creating an unfair comparison and potentially omitting relevant objects. This restriction may boost its performance but reduces its applicability in real-world scenarios, where all relevant instruments need to be segmented.

In contrast, our model, RoSIS, achieves competitive perfor-

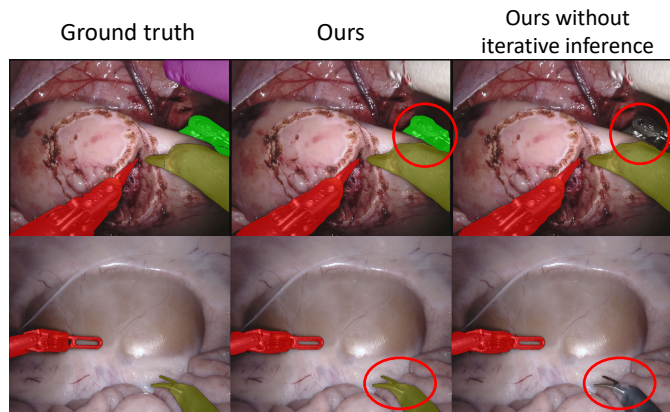


Fig. 5. Visual comparison of iterative inference strategies

TABLE IV

VISUAL AND LANGUAGE FEATURE FUSION STRUCTURAL ABLATION STUDY ON ENDOVIS2018 DATASET.

	ISI IoU	mc IoU
VLTF [15]	68.58	33.48
PWAM [12]	66.94	36.89
Ours	71.65	38.23
(+) Raw language feature	74.36 (+2.71)	41.87 (+3.64)
(+) Spatial token	66.76 (-4.89)	27.35 (-10.88)
(+) Language token	76.16 (+4.51)	44.54 (+6.31)

mance compared to S3Net with Ch IoU, ISI IoU, and mc IoU scores while operating under robust conditions. Compared to S3Net, RoSIS is designed with an end-to-end training pipeline and a straightforward inference setting. This streamlined approach makes RoSIS more suitable for practical applications, maintaining high segmentation accuracy without limiting the number of instances. Also, we evaluate other vision-based and promptable methods with RoSIS. Our method outperforms previous methods under robust conditions, has a more even overall class-wise performance distribution, and has less performance degradation for ISI IoU than for Ch IoU. This demonstrates the effectiveness of our method's fusion structure, prompt design, and iterative inference. Notably, despite the limitations imposed by a robust evaluation environment, RoSIS achieves superior performance in two instrument categories: VS with 45.32 and UP with 44.99. These results show RoSIS's capability to balance promptable and vision-based features, making it a versatile and efficient solution for surgical instrument segmentation.

3) *Ablation study of the prompt and iterative inference process*: Table III presents the ablation study results on the EndoVis2018 dataset, emphasizing the role of iterative inference and text prompts. Starting with the baseline using only the name prompt such as "The bipolar forceps," the model achieves ISI IoU and mc IoU scores of 67.74 and 37.84, respectively. Adding the location prompt to the name prompt slightly improves performance in ISI IoU. Then, the iterative inference consistently improves performance across both metrics. When applied to the location prompt configuration, iterative inference significantly boosts ISI IoU and mc IoU. This demonstrates that iterative inference effectively refines

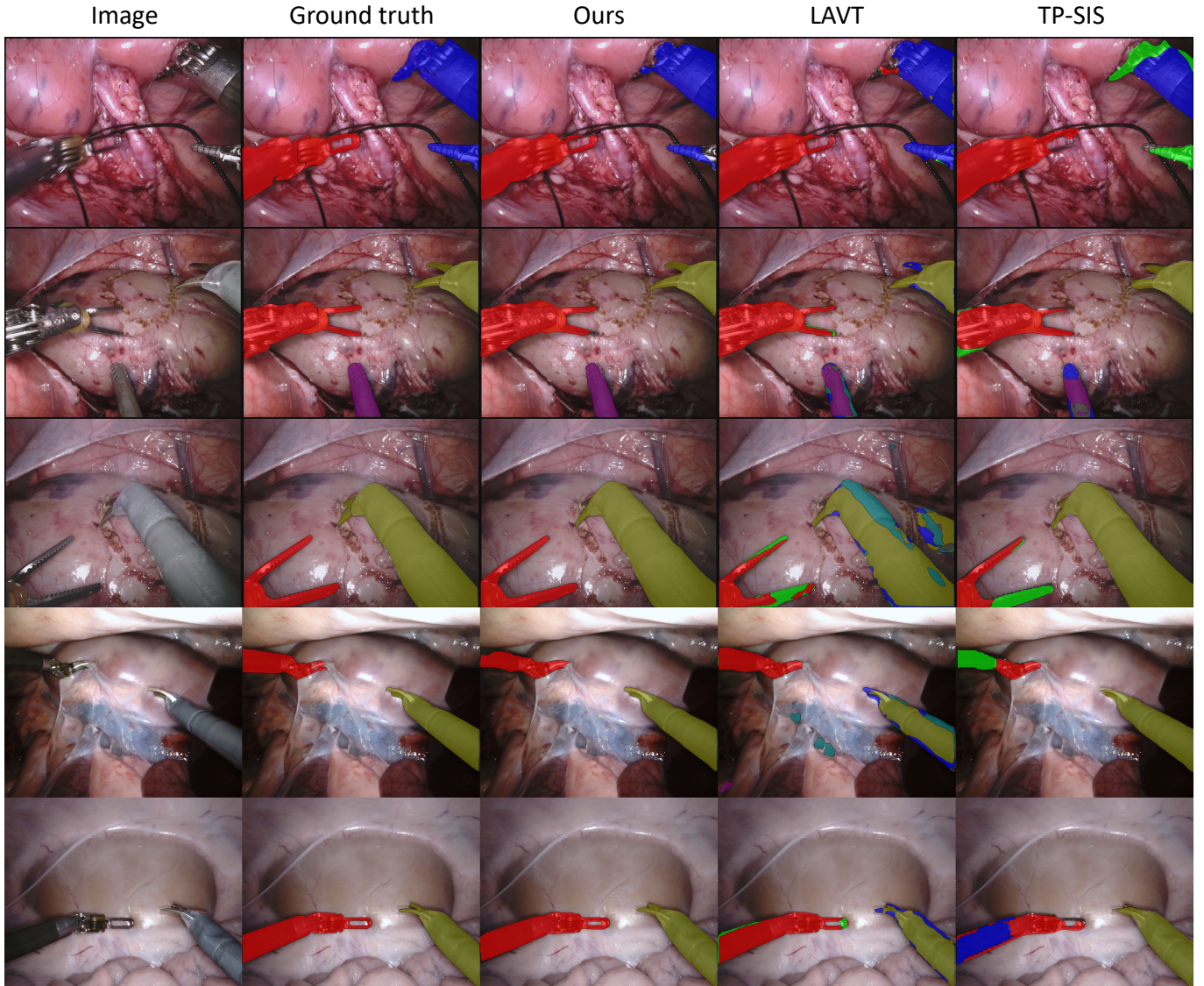


Fig. 6. Qualitative results of our predicted maps, the ground truth masks, and other promptable segmentation methods from the EndoVis2018 validation set.

the segmentation map by utilizing location-specific prompts, contributing to more accurate segmentation. Similarly, when iterative inference is incorporated with the gpt4 prompt, which provides descriptive characteristics for each instrument, there is a substantial improvement in segmentation accuracy. The ISI IoU increases by 4.79, and mc IoU increases by 3.93. This improvement shows the synergy between descriptive prompts and iterative inference, as the iterative process allows the model to refine segmentation based on more detailed object information. Also, as shown in the red circle part of Fig. 5, iterative inference allows for more accurate object segmentation maps.

These results indicate the crucial role of iterative inference in our model. By refining segmentation through multiple stages and adapting prompts based on previous outputs, iterative inference contributes to significant gains in both general and class-specific accuracy, making it a key factor in achieving optimal segmentation performance.

4) *Ablation study of the structure*: Table IV presents the results of our ablation study on the EndoVis2018 dataset, evaluating the impact of different fusion structures on the integration of visual and language features. We use ISI IoU and mc IoU as comparison metrics to focus on performance in robust settings for all ablation studies. The baseline models, VLTF [15] and PWAM [12], achieve ISI IoU scores of 68.58 and 66.94, and mc IoU scores of 33.48 and 36.89, respectively. In comparison, our model with the base fusion structure performs better, achieving an ISI IoU of 71.65 and an mc IoU of 38.23.

Further modifications demonstrate the effectiveness of specific fusion components. Adding raw language features increases ISI IoU and mc IoU to +2.71 and +3.64, respectively. The raw language feature means using the language feature from BERT [29] directly as input for the MHCA in the existence prediction branch. Additionally, incorporating spatial tokens reduces ISI IoU by -4.89 and mc IoU by -10.88,

TABLE V

CROSS-DATASET SETTING PERFORMANCE COMPARISON BY TRAINING ON THE ENDOVIS2018 AND TESTING ON THE ENDOVIS2017.

Method	Ch IoU	ISI IoU	mc IoU
LAVT [12]	40.82	14.35	13.26
TP-SIS [10]	34.23	18.57	20.16
RoSIS (ours)	42.45	34.67	27.68

suggesting that spatial tokens may introduce irrelevant spatial information, which negatively impacts performance. A spatial token refers to a structure that applies MHCA to visual features instead of language tokens in the MMFB. These results show that it is important to retain the visual features that have the original spatial and structural information from the visual encoder when performing vision-language feature fusion. Conversely, adding language tokens significantly improves results, with ISI IoU reaching 76.16 (+4.51) and mc IoU reaching 44.54 (+6.31), confirming that structured language information enhances the model’s ability to segment surgical instruments accurately.

These findings demonstrate the importance of selecting the appropriate fusion strategies. Language tokens are the most effective, providing a robust integration of language and visual features that significantly enhance segmentation performance.

5) *Qualitative results*: In Fig. 6, we visualize the prediction of our model, the ground truth, and the other promptable segmentation methods [10], [12]. Since other methods are trained without robust conditions, they hard to determine the presence or absence of objects in the R-SIS environment, resulting in higher false positives in the predicted maps. As shown in the 4th and 5th columns of Fig. 6, the segmentation masks for various classes overlap. This overlap occurs because segmentation maps are generated for all classes’ text prompts, causing all maps to merge. In contrast, our model first verifies the presence or absence of an object before generating a map, producing a clean segmentation for a single object and leading to a low false positive rate, which is crucial in surgical environments.

6) *Cross-dataset study*: We also evaluate our method in a cross-dataset setting. In this setup, the model is trained on the EndoVis2018 dataset and tested on the EndoVis2017 dataset, and vice versa. The EndoVis2017 and EndoVis2018 datasets share five common categories and each includes two unique categories. As shown in Tables 5 and 6, RoSIS demonstrates better performance compared to other promptable segmentation methods. Additionally, even among shared categories, there are slight differences in shape and domain variations, making the cross-dataset experiment indicate the generalizability of methods.

The promptable segmentation methods LAVT [12] and TP-SIS [10] show overall lower performance, with a large discrepancy between their Ch IoU and ISI IoU scores. In contrast, our method, RoSIS, achieves the best results, with a smaller gap between Ch IoU and ISI IoU, highlighting its robustness and efficiency. These results demonstrate the generalizability and effectiveness of RoSIS in handling domain shifts across different datasets.

TABLE VI

CROSS-DATASET SETTING PERFORMANCE COMPARISON BY TRAINING ON THE ENDOVIS2017 AND TESTING ON THE ENDOVIS2018.

Method	Ch IoU	ISI IoU	mc IoU
LAVT [12]	46.57	15.67	14.91
TP-SIS [10]	37.81	26.72	14.93
RoSIS (ours)	58.31	51.00	23.99

V. CONCLUSION

In this work, we presented Robust Surgical Instrument Segmentation (RoSIS), a novel framework focused on enhancing the robustness and effectiveness of text-promptable surgical instrument segmentation. Recognizing the limitations of existing methods, which often rely on assumptions about object presence, we redefined the task under robust conditions as Robust text-promptable SIS (R-SIS). RoSIS employs an encoder-decoder architecture with a Multi-Modal Fusion Block (MMFB) and a Selective Gate Block (SGB) to achieve a balanced integration of visual and language features, preventing the dominance of either modality. Additionally, we introduced an iterative inference strategy to refine segmentation maps, utilizing both name-based and location-based prompts to improve accuracy. Our experiments on the EndoVis2017 and EndoVis2018 datasets demonstrated that RoSIS outperforms existing vision-based and promptable methods under robust conditions. Ablation studies further validated the effectiveness of our fusion structures, as well as the iterative inference approach, confirming RoSIS’s adaptability across diverse surgical scenarios. This work lays a foundation for future research in multi-modal surgical instrument segmentation, with applications in other areas where vision-language integration is essential for complex surgical scene understanding.

REFERENCES

- [1] K. Fuchs, “Minimally invasive surgery,” *Endoscopy*, vol. 34, no. 02, pp. 154–159, 2002.
- [2] A. G. Harrell and B. T. Heniford, “Minimally invasive abdominal surgery: lux et veritas past, present, and future,” *The American journal of surgery*, vol. 190, no. 2, pp. 239–243, 2005.
- [3] A. A. Shvets, A. Rakhlin, A. A. Kalinin, and V. I. Iglovikov, “Automatic instrument segmentation in robot-assisted surgery using deep learning,” in *2018 17th IEEE international conference on machine learning and applications (ICMLA)*. IEEE, 2018, pp. 624–628.
- [4] V. Iglovikov and A. Shvets, “Ternausnet: U-net with vgg11 encoder pre-trained on imagenet for image segmentation,” *arXiv preprint arXiv:1801.05746*, 2018.
- [5] Y. Jin, K. Cheng, Q. Dou, and P.-A. Heng, “Incorporating temporal prior from motion flow for instrument segmentation in minimally invasive surgery video,” in *Medical Image Computing and Computer Assisted Intervention—MICCAI 2019: 22nd International Conference, Shenzhen, China, October 13–17, 2019, Proceedings, Part V 22*. Springer, 2019, pp. 440–448.
- [6] Z. Zhao, Y. Jin, X. Gao, Q. Dou, and P.-A. Heng, “Learning motion flows for semi-supervised instrument segmentation from robotic surgical video,” in *Medical Image Computing and Computer Assisted Intervention—MICCAI 2020: 23rd International Conference, Lima, Peru, October 4–8, 2020, Proceedings, Part III 23*. Springer, 2020, pp. 679–689.
- [7] C. González, L. Bravo-Sánchez, and P. Arbelaz, “Isinet: an instance-based approach for surgical instrument segmentation,” in *International Conference on Medical Image Computing and Computer-Assisted Intervention*. Springer, 2020, pp. 595–605.

- [8] B. Baby, D. Thapar, M. Chasmai, T. Banerjee, K. Dargan, A. Suri, S. Banerjee, and C. Arora, "From forks to forceps: A new framework for instance segmentation of surgical instruments," in *Proceedings of the IEEE/CVF winter conference on applications of computer vision*, 2023, pp. 6191–6201.
- [9] N. Ayobi, A. Pérez-Rondón, S. Rodríguez, and P. Arbeláez, "Matis: Masked-attention transformers for surgical instrument segmentation," in *2023 IEEE 20th International Symposium on Biomedical Imaging (ISBI)*. IEEE, 2023, pp. 1–5.
- [10] Z. Zhou, O. Alabi, M. Wei, T. Vercauteren, and M. Shi, "Text promptable surgical instrument segmentation with vision-language models," *Advances in Neural Information Processing Systems*, vol. 36, pp. 28 611–28 623, 2023.
- [11] W. Yue, J. Zhang, K. Hu, Q. Wu, Z. Ge, Y. Xia, J. Luo, and Z. Wang, "Part to whole: Collaborative prompting for surgical instrument segmentation," *arXiv preprint arXiv:2312.14481*, 2023.
- [12] Z. Yang, J. Wang, Y. Tang, K. Chen, H. Zhao, and P. H. Torr, "Lavt: Language-aware vision transformer for referring image segmentation," in *Proceedings of the IEEE/CVF Conference on Computer Vision and Pattern Recognition*, 2022, pp. 18 155–18 165.
- [13] L. Yu, Z. Lin, X. Shen, J. Yang, X. Lu, M. Bansal, and T. L. Berg, "Mattnet: Modular attention network for referring expression comprehension," in *Proceedings of the IEEE conference on computer vision and pattern recognition*, 2018, pp. 1307–1315.
- [14] C. Liu, H. Ding, and X. Jiang, "Gres: Generalized referring expression segmentation," in *Proceedings of the IEEE/CVF conference on computer vision and pattern recognition*, 2023, pp. 23 592–23 601.
- [15] J. Wu, X. Li, X. Li, H. Ding, Y. Tong, and D. Tao, "Towards robust referring image segmentation," *IEEE Transactions on Image Processing*, 2024.
- [16] J. Achiam, S. Adler, S. Agarwal, L. Ahmad, I. Akkaya, F. L. Aleman, D. Almeida, J. Altenschmidt, S. Altman, S. Anadkat *et al.*, "Gpt-4 technical report," *arXiv preprint arXiv:2303.08774*, 2023.
- [17] W. Yue, J. Zhang, K. Hu, Y. Xia, J. Luo, and Z. Wang, "Surgical-sam: Efficient class promptable surgical instrument segmentation," in *Proceedings of the AAAI Conference on Artificial Intelligence*, vol. 38, no. 7, 2024, pp. 6890–6898.
- [18] M. Allan, A. Shvets, T. Kurmann, Z. Zhang, R. Duggal, Y.-H. Su, N. Rieke, I. Laina, N. Kalavakonda, S. Bodenstedt *et al.*, "2017 robotic instrument segmentation challenge," *arXiv preprint arXiv:1902.06426*, 2019.
- [19] M. Allan, S. Kondo, S. Bodenstedt, S. Leger, R. Kadkhodamohammadi, I. Luengo, F. Fuentes, E. Flouty, A. Mohammed, M. Pedersen *et al.*, "2018 robotic scene segmentation challenge," *arXiv preprint arXiv:2001.11190*, 2020.
- [20] Z. Zhao, Y. Jin, and P.-A. Heng, "Trasetr: track-to-segment transformer with contrastive query for instance-level instrument segmentation in robotic surgery," in *2022 International conference on robotics and automation (ICRA)*. IEEE, 2022, pp. 11 186–11 193.
- [21] O. Ronneberger, P. Fischer, and T. Brox, "U-net: Convolutional networks for biomedical image segmentation," in *Medical image computing and computer-assisted intervention—MICCAI 2015: 18th international conference, Munich, Germany, October 5-9, 2015, proceedings, part III 18*. Springer, 2015, pp. 234–241.
- [22] K. He, G. Gkioxari, P. Dollár, and R. Girshick, "Mask r-cnn," in *Proceedings of the IEEE international conference on computer vision*, 2017, pp. 2961–2969.
- [23] B. Cheng, I. Misra, A. G. Schwing, A. Kirillov, and R. Girdhar, "Masked-attention mask transformer for universal image segmentation," in *Proceedings of the IEEE/CVF conference on computer vision and pattern recognition*, 2022, pp. 1290–1299.
- [24] A. Kirillov, E. Mintun, N. Ravi, H. Mao, C. Rolland, L. Gustafson, T. Xiao, S. Whitehead, A. C. Berg, W.-Y. Lo *et al.*, "Segment anything," in *Proceedings of the IEEE/CVF International Conference on Computer Vision*, 2023, pp. 4015–4026.
- [25] A. Radford, J. W. Kim, C. Hallacy, A. Ramesh, G. Goh, S. Agarwal, G. Sastry, A. Askell, P. Mishkin, J. Clark *et al.*, "Learning transferable visual models from natural language supervision," in *International conference on machine learning*. PMLR, 2021, pp. 8748–8763.
- [26] H. Ding, C. Liu, S. Wang, and X. Jiang, "Vision-language transformer and query generation for referring segmentation," in *Proceedings of the IEEE/CVF International Conference on Computer Vision*, 2021, pp. 16 321–16 330.
- [27] G. Feng, Z. Hu, L. Zhang, and H. Lu, "Encoder fusion network with co-attention embedding for referring image segmentation," in *Proceedings of the IEEE/CVF Conference on Computer Vision and Pattern Recognition*, 2021, pp. 15 506–15 515.
- [28] A. Dosovitskiy, "An image is worth 16x16 words: Transformers for image recognition at scale," *arXiv preprint arXiv:2010.11929*, 2020.
- [29] J. Devlin, "Bert: Pre-training of deep bidirectional transformers for language understanding," *arXiv preprint arXiv:1810.04805*, 2018.
- [30] Z. Liu, Y. Lin, Y. Cao, H. Hu, Y. Wei, Z. Zhang, S. Lin, and B. Guo, "Swin transformer: Hierarchical vision transformer using shifted windows," in *Proceedings of the IEEE/CVF international conference on computer vision*, 2021, pp. 10 012–10 022.
- [31] X. Zhu, W. Su, L. Lu, B. Li, X. Wang, and J. Dai, "Deformable detr: Deformable transformers for end-to-end object detection," *arXiv preprint arXiv:2010.04159*, 2020.
- [32] T.-Y. Lin, P. Dollár, R. Girshick, K. He, B. Hariharan, and S. Belongie, "Feature pyramid networks for object detection," in *Proceedings of the IEEE conference on computer vision and pattern recognition*, 2017, pp. 2117–2125.
- [33] A. Paszke, S. Gross, F. Massa, A. Lerer, J. Bradbury, G. Chanan, T. Killeen, Z. Lin, N. Gimelshein, L. Antiga *et al.*, "Pytorch: An imperative style, high-performance deep learning library," *Advances in neural information processing systems*, vol. 32, 2019.
- [34] J. Deng, W. Dong, R. Socher, L.-J. Li, K. Li, and L. Fei-Fei, "Imagenet: A large-scale hierarchical image database," in *2009 IEEE conference on computer vision and pattern recognition*. Ieee, 2009, pp. 248–255.
- [35] I. Loshchilov, "Decoupled weight decay regularization," *arXiv preprint arXiv:1711.05101*, 2017.